FULL PAPER

Hierarchical Intrafibrillar Nanocarbonated Apatite Assembly Improves the Nanomechanics and Cytocompatibility of Mineralized Collagen

Yan Liu, Dan Luo, Xiao-Xing Kou, Xue-Dong Wang, Franklin R. Tay, Yin-Lin Sha, Ye-Hua Gan,* and Yan-Heng Zhou*

Nanoscale replication of the hierarchical organization of minerals in biogenic mineralized tissues is believed to contribute to the better mechanical properties of biomimetic collagen scaffolds. Here, an intrafibrillar nanocarbonated apatite assembly is reported, which has a bone-like hierarchy, and which improves the mechanical and biological properties of the collagen matrix derived from fibril-apatite aggregates. A modified biomimetic approach is used, which based on the combination of poly(acrylic acid) as sequestration and sodium tripolyphosphate as templating matrix-protein analogs. With this modified dual-analog-based biomimetic approach, the hierarchical association between collagen and the mineral phase is discerned at the molecular and nanoscale levels during the process of intrafibrillar collagen mineralization. It is demonstrated by nanomechanical testing, that intrafibrillarly mineralized collagen features a significantly increased Young's modulus of 13.7 ± 2.6 GPa, compared with pure collagen (2.2 ± 1.7 GPa) and extrafibrillarly-mineralized collagen (7.1 ± 1.9 GPa). Furthermore, the hierarchy of the nanocarbonated apatite assembly within the collagen fibril is critical to the collagen matrix's ability to confer key biological properties, specifically cell proliferation, differentiation, focal adhesion, and cytoskeletal arrangement. The availability of the mineralized collagen matrix with improved nanomechanics and cytocompatibility may eventually result in novel biomaterials for bone grafting and tissue-engineering applications.

Dr. Y. Liu, Dr. X.-X. Kou, Dr. X.-D. Wang,
Prof. Y.-H. Zhou
Department of Orthodontics
Peking University School and Hospital of Stomatology
Beijing 100081, P. R. China
E-mail: yanhengzhou@gmail.com
Dr. D. Luo, Prof. Y.-L. Sha
Single-molecule and Nanobiology Laboratory
Department of Biophysics
School of Basic Medical Sciences and Biomed-X Center
Peking University
Beijing 100191, P. R. China
Prof. F. R. Tay
Department of Endodontics
Georgia Health Sciences University
Augusta, Georgia 30912, USA
Prof. Y.-H. Gan
Central Laboratory
Department of Oral and Maxillofacial Surgery
Peking University School and Hospital of Stomatology
Beijing 100081, P. R. China
E-mail: kqyehuagan@bjmu.edu.cn

1. Introduction

Biogenic mineralized tissues, such as those found in bones and teeth, possess specific mechanical properties required to resist different forces and stresses due to the hierarchical arrangement of carbonated hydroxyapatites within collagen fibrils (i.e., intrafibrillar mineralization) at the molecular and nanoscale levels.[1,2] The intrafibrillar carbonated hydroxyapatites are predominantly located inside the gap zones between abutting collagen molecules during the early stages of biomineralization, and extend into the intermolecular spaces between adjacent collagen molecules but within collagen fibrils (i.e., overlap zones) during the later stages of biomineralization.[3–7] The higher density of carbonated hydroxyapatite crystallites in the gap zones of individual mineralized fibril gives rise to a periodic banding pattern (ca. 67 nm), with the repeat motif corresponding to the *D*-period (i.e., tropocollagen molecules staggered from each other by about 67 nm) of the unmineralized collagen fibril.[8–10] This intriguing biological process has inspired scientists to mimic its mechanism for fabricating mineralized collagen matrices with similar hierarchy for bone grafting and tissue engineering.

From earlier research reporting the deposition of apatite crystallites around collagen fibrils (i.e., extrafibrillar mineralization),[11,12] to more recent research demonstrating intrafibrillar mineralization within collagen fibrils,[7,13] biomineralization events have been better understood over the past decade. With the recent identification of amorphous precursors in biogenic mineralized tissues in vivo, the debate for the occurrence of biomineralization via a transient amorphous precursor is tempered.[14,15] As acidic non-collagenous proteins play an important role in facilitating amorphous precursors,[16] polyanionic polymers such as poly(aspartic acid) or poly(acrylic acid) (PAA) have been employed as sequestration analogs of those non-collagenous proteins to attain intrafibrillar mineralization.[17–23] The role of the polymers in those studies is to suppress bulk crystallization and to stabilize the amorphous phase. However, the application of only a sequestration analog results in

www.MaterialsViews.com

ADVANCED
FUNCTIONAL
MATERIALS
www.afm-journal.de

FULL PAPER

non-hierarchical intrafibrillar mineralization, which fails to reproduce the hierarchy of apatite assembly (i.e., overlapping platelets producing periodic bands) in biogenic mineralized tissues.[19,20,23] Furthermore, the absence of 67 nm periodic bands in a fibril suggest the mineralization process may not be compatible with physiological fibrillogenesis.[22] As dual sequestration and nucleation functions contributed by specific domains of non-collagenous proteins are revealed in biomineralization processes,[24,25] a biomimetic approach based on the combination of a precursor sequestration motif and an apatite templating motif of these proteins has therefore been developed to induce hierarchical intrafibrillar mineralization of preformed single-layer collagen fibrils at the nanoscale in our previous studies.[26–28] However, the impact of this hierarchical intrafibrillar mineralization on the biofunctions of fibrillar biomaterials in tissue engineering has not been investigated. We hypothesized that hierarchical nanocarbonated apatite assembly within a collagen fibril may enhance the mechanical and biological properties of collagen matrices made of fibril-apatite aggregates.

In the present study, hierarchical intrafibrillar mineralization was achieved using a modified dual-analog-based biomimetic approach,[26–28] allowing formation of bone-like structure at the molecular and nanoscale levels. In this strategy, self-assembly of triple-helical tropocollagen molecules into fibrils and hierarchical arrangement of stabilized amorphous nanoprecursors in the gap zones of fibrils occurred simultaneously, although this process may not fully mimic the way the natural bone formation occurs. To test the hypothesis that the hierarchical intrafibrillar nanocarbonated apatite assembly could improve the nanomechanics and cytocompatibility of collagen matrices made of fibril-apatite aggregates, we tested the Young's modulus of collagen at the nanoscale, and the biomedical potential of the collagen, such as cellular viability, differentiation capacity, focal adhesion, and cytoskeletal arrangement.

2. Results and Discussion

2.1. Hierarchical Intrafibrillar Nanocarbonated Apatite Assembly and Characterization

As structural organization of collagen molecules and fibrils is an essential prerequisite for their subsequently mineralization,[29] we thus first tested the ability of collagen molecules to assemble into collagen fibrils in simulated body fluid (SBF), using atomic force microscopy (AFM) (**Figure 1**). Initially, rod-like collagen molecules adsorbed to mica and formed a disordered mesh within 30 min (Figure 1A). After 1 h, the molecules (5–8 strands) were combined by overlapping and intertwining with each other to form higher-order microfibrils with width of 23.8 ± 4.3 nm, which, in turn, aggregated longitudinally and laterally with adjacent microfibrils to form collagen fibrils (149.5 ± 32.6 nm in width) within 4 h, and nanofibers (265.0 ± 52.7 nm in width) within 24 h.[30] Both fibrils and nanofibers possessed distinct D-periods with 67 nm (Supporting Information, Figure S1,S2). This data confirms that the assembly of unidirectionally aligned fibril occurs in a native-like manner
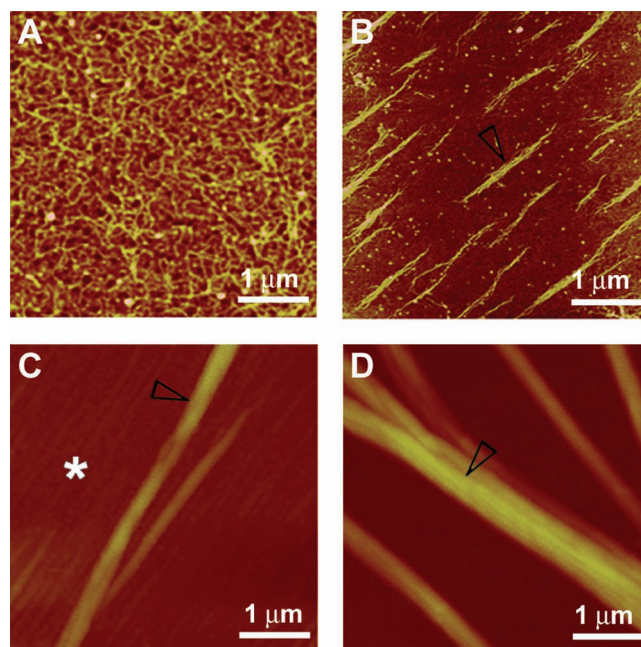

Figure 1. Collagen assembly on muscovite mica, observed by AFM. All of the images were taken from reconstitution with 10 µg mL⁻¹ tropocollagen solution at pH 5. A) 30 min of incubation, showing randomly adsorbed collagen molecules. B) 1 h of incubation, showing the emergence of microfibrils (5–8 strands, open arrowhead) aligned in parallel. C) 4 h of incubation, showing the emergence of fibrils with faint D-periods (ca. 67 nm). Open arrowhead: staggered arrangement of two fibrils; asterisk: underlying microfibrils (56.8 ± 10.9 nm in width) aligned in parallel. D) 24 h of incubation, showing nanofibers with distinct D-periods (265.0 ± 52.7 nm in width, open arrowhead).

in the absence of cells.[31] The morphology of the formed layer depended on the incubation time of the tropocollagen solution on mica, which was very similar to a previous AFM study.[32]

To develop hierarchical, intrafibrillarly mineralized collagen (IFM), we used a modified dual-analog-based biomimetic approach, in which self-assembly of triple-helical tropocollagen molecules into fibrils and hierarchical arrangement of PAA-stabilized amorphous calcium phosphate (ACP) in the gap zones of fibrils occurred simultaneously in the presence of sodium tripolyphosphate (TPP)[26] as a templating analog. **Figure 2**A shows the presence of mineral phase in both the gap zones between abutting collagen molecules, and the intermolecular spaces between adjacent collagen molecules, within 4 h of mineralization. After 24 h, the fibrils aggregated into intertwined nanofibers (247.7 ± 43 nm in width), with distinct banding pattern observed by AFM (Figure 2C). Combined with AFM, transmission electron microscopy (TEM) was used to assess the nanostructure of mineralized fibrils without staining (Figure 2B,D). The corresponding mineral phase was evaluated by selected area electron diffraction (SAED) coupled to TEM. The TEM showed the process of incorporation of nano-ACPs into the fibril (open arrows in Figure 2B), and the increasingly distinct banding pattern (ca. 67 nm) in the electron-dense nucleation sites corresponding to the D-period of collagen molecules (open arrowheads in Figure 2B). The nano-ACP phase was
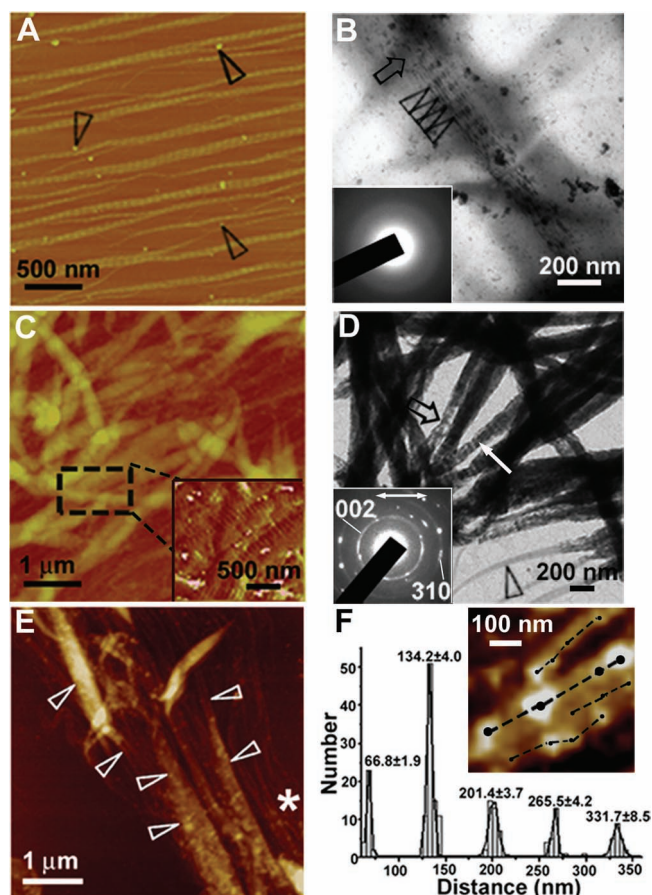
ADVANCED
FUNCTIONAL
MATERIALS
www.afm-journal.de

Materials
Views
www.MaterialsViews.com

Figure 2. Intrafibrillar mineralization of collagen in the presence of two biomimetic analogs, observed by AFM (A,C,E) and TEM (B,D). A) 4 h of mineralization, showing assembly of paralleled microfibrils (43.9±10.5 nm in width), side by side. Precipitation of nano-ACP (30.2 ± 5.1 nm in diameter) into both the gap zones and the intermolecular spaces within the fibrils (open arrowheads) occurred simultaneously. B) Corresponding unstained TEM image of mineralization for 4 h, showing nanophases (open arrow) that aggregated along the fibrillar surface, and increasingly apparent cross-banding corresponding to the D-periods of collagen molecules (open arrowheads). SAED (inset) indicating the mineral phase was predominantly amorphous. C) 24 h of mineralization, showing mineralized nanofibers (247.7 ± 43 nm in width). Inset: phase image of the rectangle in (C), showing distinct D-periods. D) Corresponding unstained TEM image of mineralization for 24 h, showing nanofibers with high electron density. Some mineralized fibrils with crystals in face-on orientation showed obvious D-periods (arrow), while the fibrils with crystals in edge-on orientation didn't exhibit periodic changes of the mineral density (open arrow). SAED (inset) of the intrafibrillar nanocrystals indicate distinct arc-shaped patterns characteristic of carbonated apatite. The orientation of the carbonated apatite (002) reflection was parallel to the 67 nm collagen reflection (arrow), which demonstrates that the crystalline c axes and the axial direction of the mineralized fibril (double arrows) were aligned. Open arrowhead: unmineralized fibril showing dehydration shrinkage. E) 16 h of mineralization, showing that ACP droplets in the intermolecular spaces promoted aggregation of the collagen nanofibrils (48.2 ± 3.9 nm in width) or the formation of collagen fibrils (144.4 ± 16.3 nm in width) or bundles (311.5 ± 53.6 nm in width) (open arrowheads). F) Calculation of the distance between each two abutting ACP droplets (Inset: higher magnification of the mineralized fibril from the asterisked region in (E)). The data are shown as mean ± SD. Interestingly, the fitted data were very close to 67 nm or multiplies of 67 nm, corresponding to the D-period of the collagen molecules.

subsequently transformed into a more closely packed nanocrystalline phase, as revealed by SAED (Figure 2D). In this stage, collagen fibrils were heavily mineralized with intrafibrillar nanocarbonated apatites, reproducing the periodic banding pattern of naturally mineralized collagen.[33] The complementary use of AFM and TEM enabled us to demonstrate the sequence of mineralizing reactions and fibrillar nanostructures.

Although there are many reports on fabrication of bone-like structures,[17–23,26–28] the intriguing interplay between collagen and mineral phase during mineralization at the molecular and nanoscale levels has never been explored. In this work, the 16 h-fibrillized collagen revealed this intricate interaction. We found that the more ACP droplets there were in the intermolecular spaces, the more or the wider were the microfibrils (48.2 ± 3.9 nm in width) (open arrowheads in Figure 2E). Those results implied that ACP droplets could promote the aggregation of collagen microfibrils or the formation of collagen nanofibers (311.5 ± 53.6 nm in width). Further, we calculated the distance between every two abutting ACP droplets (n = 200) and analyzed the data using multipeaks Gaussian fitting technique (Figure 2F). The fitted data showed that the distance between two droplets was almost identical to 67 nm or multiplies of 67 nm, principally corresponding to the D-periods of collagen molecules. This data provided direct visual evidence of the location of the mineral phase in association with collagen, as has been shown in naturally mineralized tissues.[34] However, this periodic arrangement of mineral phase could not be discerned in the extrafibrillarly mineralized collagen (EFM). Therefore, the hierarchical nanocarbonated apatite assembly identified within the IFM may be attributed to the templating function of the nucleation analog of matrix phosphoproteins (i.e., TPP). This confirms the important role of natural matrix proteins in biomineralization of vertebrate collagenous tissues in vivo.[16]

In the absence of the two biomimetic analogs, ACP spherules (ca. 50–100 nm in diameter) formed around collagen fibrils (**Figure 3**A,B), and transformed into needle-shaped carbonated apatites (ca. 250 nm in length) that were randomly precipitated over the surface of collagen fibrils after 24 h (Figure 3C,D). Implicit in the results is that the ordered mineralization of collagen fibrils cannot be achieved without biomimetic analogs.[11,12] Although infiltration of stabilized ACPs into collagen could be also attained without the nucleation analog, the periodic banding pattern could not be identified even in sparsely mineralized fibrils.[26] This phenomenon further confirms the important role of dual sequestration and nucleation functions of non-collagenous proteins in reproducing hierarchical mineral arrangement within a collagen fibril.[35]

2.2. Nanomechanical Analysis by PeakForce QNM AFM

To evaluate the influence of hierarchy of nanocarbonated apatite assembly on the mechanical properties of collagen, we compared the Young's modulus of pure collagen, EFM and IFM at the nanoscale, using a recently developed AFM surface property mapping technique: PeakForce QNM AFM. PeakForce tapping provides high-resolution mapping of the nanomechanical properties for each sample, and exerts a maximum force control of
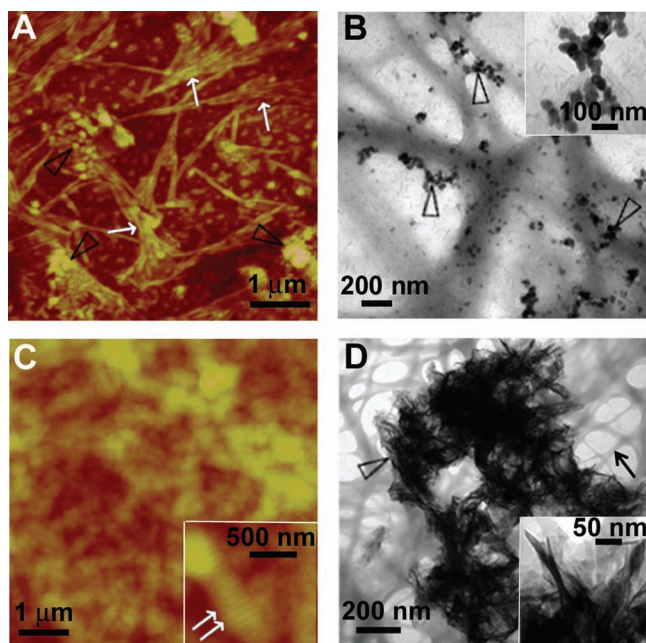
Figure 3. Extrafibrillar mineralization of collagen in the absence of two biomimetic analogs, observed by AFM (A,C) and TEM (B,D). A) 4 h of mineralization, showing randomly arranged fibrils without periodic bands (arrows). Open arrowheads: ACP precursors (63.7 ± 15.2 nm in diameter) aggregate into large clusters outside the fibrils. B) Corresponding unstained TEM image of mineralization for 4 h. The ACP precursors (open arrowheads) are arranged around the fibrils. Inset: ACP nanoparticles (ca. 50–100 nm in diameter). C) 24 h of mineralization. Inset: carbonated apatite clusters arranged around the fiber (ca. 400 nm in width) with obvious D-periods (arrows: ca. 67 nm). D) Corresponding unstained TEM image of mineralization for 24 h. Spherules of needle-shaped carbonated apatites (inset: ca. 250 nm in length) coated the surface (open arrowhead) of the unmineralized collagen fibrils (arrow).

Figure 4. Nanomechanical properties of collagen tested by AFM-based PeakForce QNM. All of the samples were scanned under dehydrated conditions. A) Property map of Young's modulus of a representative collagen sample. Between the arrows is a single collagen nanofiber with a low modulus. Asterisk: mica base. B) Property map of Young's modulus of a representative EFM sample. Cross-banding could be identified in some fibrils with a different distribution of moduli (open arrowhead versus arrows). C) Property map of Young's modulus of a representative IFM sample, showing the uniform distribution of the modulus. Between the arrows is a single intrafibrillarly mineralized collagen nanofiber showing distinct cross-banding. Asterisk: mica base. D) Box plot of the Young's modulus of collagen (A), EFM (B) and IFM (C) (each box plot represent the minimum, first quartile, median, third quartile, and maximum of 100 values (2 scans × 10 ROIs × 5 samples)). The different lower case letters beneath each of the box denote significant differences in the modulus distribution among the three groups.

the sample while eliminating lateral forces.[36] In addition, the maximum force exerted on the sample is maintained as constant, which is beneficial for delicate biological samples.[37,38] Using the Derjaguin–Muller–Toporov (DMT) model as the analysis software,[39] the absolute modulus of each sample could be acquired by calibration of the tip radius and spring constant.

From the PeakForce QNM AFM images in panels A to C in **Figure 4**, the representative sample from each group possessed a different modulus distribution. Obviously, pure collagen possessed the lowest modulus, and those fibrils with hierarchical intrafibrillar nanocarbonated apatite assembly reinforced the collagen to the greatest extent. The mechanism for modulus improvement is that the nanocrystalline carbonated apatites substitute water in the gap zones between the collagen molecules and establish intermolecular chemical interactions between the organic and mineral phase.[40] Trebacz and Wójtowicz have shown that the presence of a mineral can protect natural bone tissues from degradation.[41] On the contrary, unmineralized collagen was susceptible to denaturation and lost the regular D-periods (ca. 67 nm) of native collagen (Supporting Information, Figure S1). From the quantitative data in Figure 4D, the modulus of the dehydrated collagen fibrils ranged from 0.2 GPa to 7.8 GPa, which is in good agreement with a previous result
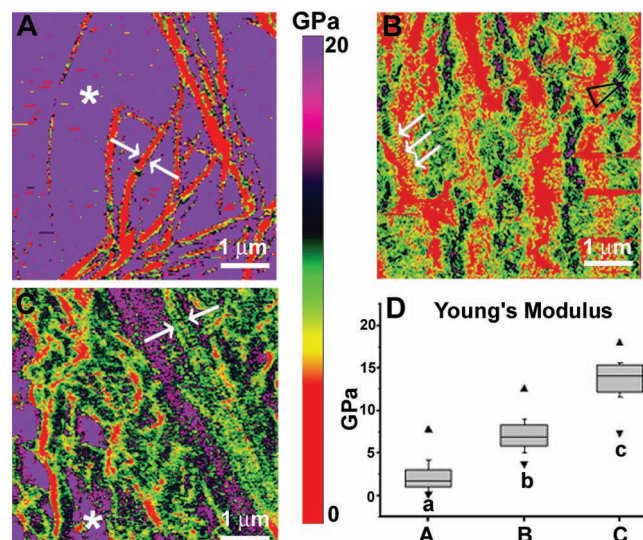
acquired by AFM-based microtensile testing.[42] Compared with EFM, with a modulus of 7.1 ± 1.9 GPa, the modulus of IFM (13.7 ± 2.6 GPa) was much higher. This result is similar to what is shown in biogenic mineralized matrices: their mechanical properties are dependent upon the hierarchically arranged intrafibrillar carbonated apatite minerals within the gap zones of the fibrils, even though extrafibrillar carbonated apatites constitute as much as 75% of the mineral phase in mineralized collagen.[43,44] Taken together, our results highlight the biomechanical significance of highly ordered intrafibrillar collagen mineralization.[1,2,45] With the application of the modified dual-analog-based biomimetic approach to more densely packed collagen scaffolds in bone-graft and tissue engineering, mineralized collagen matrices with hierarchical intrafibrillar nanocarbonated apatite assembly may be fabricated. The latter should exhibit better load-bearing properties during function, when compared with non-mineralized and extrafibrillarly mineralized collagen scaffolds.

2.3. Analyses of Cellular Biocompatibility and Morphology

Scaffolds fabricated from biological materials promise a better biomedical potential in tissue engineering, providing that
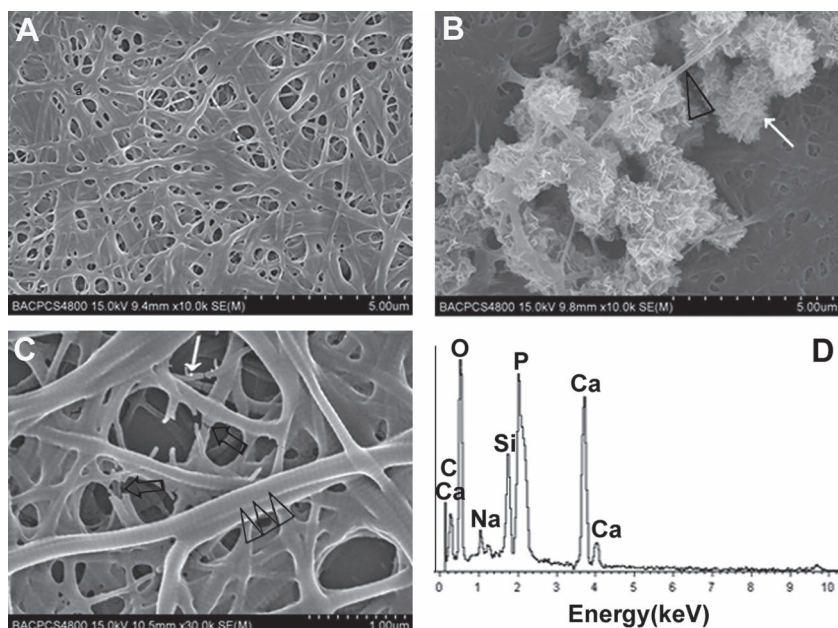
Figure 5. Scanning electron microscopy of 3D fibrillar matrices. A) Woven-like collagen matrix. B) EFM. Only flower-like (arrow: ca. 2 μm in diameter), spherulitic aggregates were deposited in the vicinity of the collagen matrix. Open arrowhead: unmineralized collagen fibril. C) IFM: in the presence of two biomimetic analogs, periodic banding patterns could vaguely be discerned along the surface of some mineralized fibrils (open arrows). Arrow: extrafibrillar nanocarbonated apatites; open arrowheads: brittle fracture. D) EDS analysis, confirming an intrafibrillar calcium phosphate mineral phase (Ca/P = 1.62) in C. Combined with the TEM-SAED data in Figure 2D, this result suggests that the intrafibrillar mineral phase was calcium-deficient carbonated apatite similar to that present in natural bone.

In the next set of experiments on cell adhesion and morphology, MG63 cells were immunostained for vinculin to label focal adhesion points (FAPs), and F-actin (phalloidin) to label the cytoskeletal arrangement. From the fluorescent microscopic images, the highest density of FAPs was observed on the surface of IFM, while the cells on the surface of glass cover-slip (control) failed to form mature focal contacts (Figure 6C). The formation of mature FAPs in the IFM indicates that the cell contacted well with the underlying scaffolds (Supporting Information, Figure S3). The reorganization of actin filaments resulting from the formation of FAPs was also pronounced in the IFM, where concentrated intertwined stress fibers formed at the cellular periphery. From thin actin fibrils in the control to the formation of specific stress fibers in different matrices (Supporting Information, Figure S4), the spatial reorganization of the actin cytoskeleton appears to be one of intracellular signals that simulate osteoblastic differentiation.[47] These great advantages of IFM in cellular behavior may be attributed to the hierarchical nanostructure of IFM, similar to native extracellular matrix in vivo.

3. Conclusions

In summary, we have found that IFM, with bone-like hierarchical nanostructures, possesses better mechanical and biological properties compared with pure collagen and EFM. The hierarchical intrafibrillar mineralization in this work was achieved using a modified biomimetic approach that involves the synchronized supplement of sequestration and nucleation biomimetic analogs. With this strategy, we demonstrate the principle of hierarchical mineralization within a fibril at the molecular and nanoscale levels. The ACP nanodroplets promote aggregation of microfibrils or the formation of nanofibers; the microfibrils, in turn, direct regular arrangement of nanodroplets in periodically spaced gap zones or intermolecular spaces. The highly ordered mineralized collagen matrix, with improved mechanical and biological properties, provides valuable information on fabrication of biomimetic collagen scaffolds for bone-grafting and tissue-engineering applications. Future research should be directed toward producing more densely packed 3D fibrillar matrices with hierarchical intrafibrillar nanocarbonated apatite assemblies, and nanoscopic dynamic mechanical analyses of those matrices under hydrated conditions.

characteristic features are preserved. Different collagen matrices prepared from highly concentrated fibrillar suspensions (1 mg mL^{-1}) were tested for their ability to support cell growth and differentiation in vitro, using an osteoblast-like cell line MG63. Before cell seeding, the morphology of the matrix was observed by scanning electron microscopy (SEM) to ensure uniform coverage of fibrils on polylysine-coated cover slips (**Figure 5**). For EFM, flower-like minerals deposited over the surface, while smooth fibrils with *D*-periodic bands were formed in the IFM. The presence of an intrafibrillar carbonated apatite mineral phase[46] in IFM was confirmed using energy dispersive X-ray spectroscopy (EDS) coupled to SEM.

Cell growth on different scaffolds was quantified using a colorimetric 3-(4,5-dimethylthiazol-2-yl)-5-(3-carboxymethoxyphenyl)-2-(4-sulfophenyl)-2H-tetrazolium (MTS) test, in which the IFM had a better cell compatibility to MG63 on days 1 and 3, compared with the control, pure collagen, and EFM (**Figure 6**A). A similar cell proliferation rate on day 7 indicates that the cells on the different scaffolds reached confluence and began to differentiate along an osteogenic lineage. As a marker of early osteoblastic differentiation, the alkaline phosphatase (ALP) activity was tested after cell seeding on days 3, 7, and 14 (Figure 6B). The ALP activity was highest on the IFM at every time point, irrespective of whether osteogenic supplements were present in the cell-culture medium. This result indicates that the hierarchy of the nanocarbonated apatite assembly within the collagen fibril could actively influence the differentiating capability of MG 63.

4. Experimental Section

Hierarchical Intrafibrillar Nanocarbonated Apatite Assembly: Based on our previously established protocol for biomimetic mineralization,[26–28] hierarchical nanocarbonated apatite assembly within a collagen fibril was achieved by the following adapted procedure: Type-I tropocollagen from
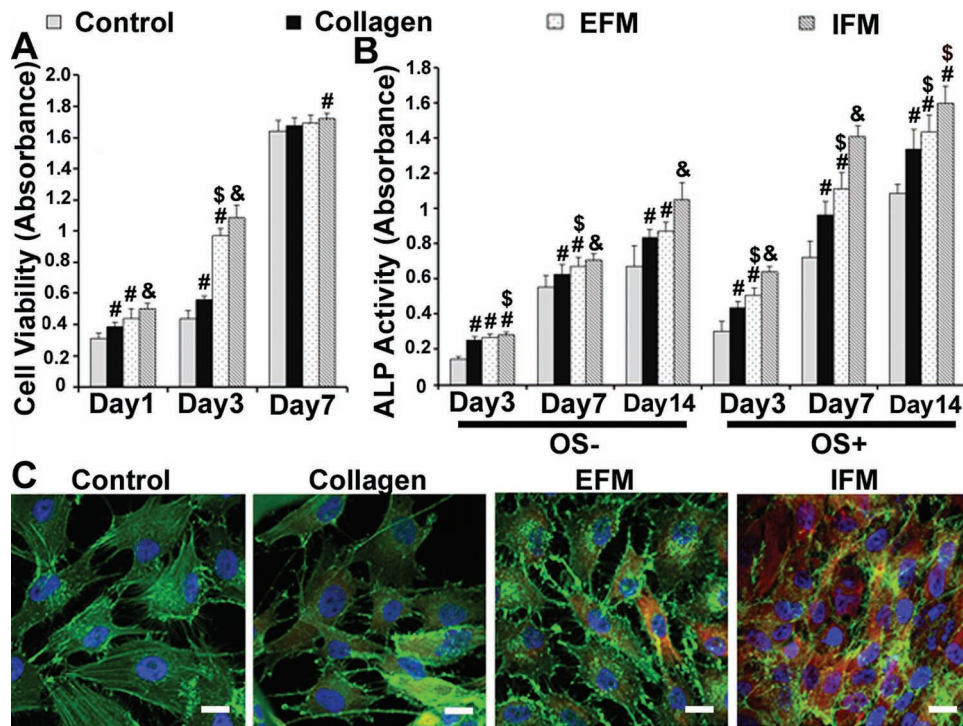
www.MaterialsViews.com

ADVANCED
FUNCTIONAL
MATERIALS
www.afm-journal.de

FULL PAPER

Figure 6. Cell-culture experiments on 3D fibrillar matrices. A) Results as a function of time of the CellTiter 96 assay indicating proliferation of MG 63 on different substrates. B) Alkaline phosphate production from MG63 cultured on different substrates as a function of time. #: $\alpha < 0.05$ versus control; $: $\alpha < 0.05$ versus collagen; &: $\alpha < 0.05$ versus all of the other groups, by ANOVA. The bars show the mean ± SD. OS−: complete medium in the absence of osteogenic supplements. C) Fluorescent microscopy images of MG 63 cultured on different scaffolds. Green represents actin filaments, red represents FAPs, and blue represents cell nuclei. Scale bar = 20 µm.

rat tails (BD Biosciences) was prepared to a collagen stock solution at a concentration of 1.98 mg mL^{-1} in acetic acid (0.1 M, pH 2.5) at 4 °C, and was used for experiments within 3 months. The stock solution was diluted to a given concentration with a phosphate source (i.e., SBF), which contained 136.8 mM NaCl, 4.2 mM NaHCO$_3$, 3.0 mM KCl, 1.0 mM K$_2$HPO$_4$·3H$_2$O, 1.5 mM MgCl$_2$·6H$_2$O, 2.5 mM CaCl$_2$, 0.5 mM Na$_2$SO$_4$, and 3.08 mM Na$_3$N. A composite disk placed in a trans-well plate (0.4 µm, Corning-Costar) released calcium and hydroxyl ions in the presence of SBF and the pH increased from 5 to 9.5.[28] Additionally, two biomimetic analogs were used to mimic the dual functions of non-collagenous proteins involved in biomineralization processes.[24,25] Specifically, PAA (0.28 mM, molecular wieght (MW) = 1800 g mol^{-1}, Sigma–Aldrich), the sequestration analog, was added to SBF to stabilize ACP as a nanoprecursor; TPP (2.5 wt%, MW = 367.9 g mol^{-1}, Sigma–Aldrich), the templating analog, was used to dialyze the stock solution to template the hierarchical arrangement of carbonated apatite within the collagen fibrils.[26] All of the reactions were performed at 37 °C for a given amount of time in a moisture chamber to minimize evaporation. Under these conditions, collagen fibril assembly and the formation of nanocrystalline carbonated apatite platelets occurred simultaneously.

Atomic Force Microscopy (AFM): Fibrillized collagen was collected on freshly cleaved muscovite mica disks (grade V1, Ted Pella Inc.) at a given time. The samples were flushed three times with deionized water in multiple flow directions and left to air-dry for more than 10 min in ambient conditions (room temperature). AFM measurements were performed in tapping mode in air using a MultiMode IV scanning probe microscope (Veeco, USA) and silicon tips (spring constant 40 N m^{-1}, freq. 300 kHz, RTESP, Veeco) with imaging speeds between 0.3 and 0.5 Hz and a 0° scan angle. The acquired images (512 × 512) were analyzed using NanoScope Version 6.12. The 24 h-fibrillized collagen was used for subsequently nanomechanical testing.

Transmission Electron Microscopy (TEM): TEM was carried out using a JEM-100CX at 100 kV. The samples were deposited on Formvar carbon-coated nickel grids without staining.

Scanning Electron Microscopy (SEM): SEM was carried out using a Hitachi S-4800 at 15 kV. All of the samples were fixed on polylysine-coated cover slips and sputter-coated with gold. Cell-seeded scaffolds were previously washed three times with phosphate buffered saline (PBS) and fixed in 3.7% methanal in PBS. After dehydration in a graded series of ethanol, the samples were critical-point dried and sputter-coated with gold for 2 min at 20 mA. EDS was coupled to the SEM.

Nanomechanical Measurements: Quantitative mechanical characterization was determined using a Bruker MultiMode 8 scanning probe microscope, operated under peak-force tapping mode with 1.0 Hz scan rates and a 200 mV amplitude set point.[36] The silicon tip (RTESP, Veeco, USA) was irradiated with UV light to remove any organic contaminates before use. Spring-constant calibration was performed by means of thermal-noise spectra in air,[48] and the spring constant was determined as 25.89 N m^{-1}. To calculate the Young's modulus, the retract curve of the force versus separation plots could be fitted by the DMT model:[39]

$$F - F_{adh} = \frac{4}{3} \; E^* \sqrt{R(d - d_0)^3}$$

where $F - F_{adh}$ is the force on the cantilever relative to the adhesion force, R is the tip radius, $d - d_0$ is the deformation of the sample, and E^* is the reduced modulus. Each set of Young's modulus measurements on a sample corresponded to 512 × 512 force–separation curves obtained over an area 5.6 µm × 5.6 µm.

Cell Culture: A human osteoblast-like MG 63 cell line obtained from American Type Culture Collection (ATCC, Rockville, MD) was used for the cytocompatibility test. Cells were cultured in Alpha Modification of Eagles Medium (α-MEM) supplemented with 10% fetal bovine serum

FULL PAPER

(FBS), and 1% penicillin/streptomycin. The collagen scaffolds were collected on polylysine-coated cover slips of 15 mm diameter, and cross-linked with 1-ethyl-3-(3-dimethylaminopropyl)-carbodiimide (0.3 M)/N-hydroxysuccinimide (0.06 M) to stabilize the scaffolds.[27] The cross-linked scaffolds were placed in a 24-well nontreated polystyrene plate with a stainless-steel ring to prevent swelling. Polylysine-coated cover slip was used as a control. All of the samples were sterilized under UV light for 2 h, washed with PBS for 15 min each to remove any residual solvent, and subsequently immersed in complete medium (α-MEM/10% FBS/1% penicillin/streptomycin) overnight before cell seeding. The isolated cells were seeded on the scaffolds at a cell density of 2×10^4 cells per well and cultured for 14 days with the medium refreshed every other day.

Cell Titer and ALP Activity: Cell proliferation on the scaffolds was determined using a colorimetric MTS assay (CellTiter 96 Aqueous One solution, Promega, Madison, WI) on days 1, 3, and 7. The osteogenic differentiation of MG63 was determined by the ALP activity. After 24 h of cultivation, the cell-culture medium of half of the samples was supplemented with 1×10^{-7} M dexamethasone, 10 mM β-glycerophosphate, and 0.05 mM ascorbic acid 2-phosphate (osteogenic supplements = OS+). The ALP activity was analyzed using the ALP Yellow Liquid scaffold system for enzyme-linked immunosorbent assay (ELISA) (Sigma Life Sciences, USA) at days 3, 7, and 14. Quantification was performed with a microplate reader according to the manufacturer's protocol.

Focal Adhesion and Cytoskeleton Staining: After 5 days of cultivation, cells were fixed in 3.7% methanal solution in PBS for 10 min, permeabilized with 0.2% Triton-X-100 and incubated with anti-vinculin antibody (Clone hVIN1, #V9264, Sigma Life Sciences) at a 10 μg mL^{-1} final concentration for 1 h. The cells were then rinsed and incubated with Alexa Fluor 488 Phalloidin (Sigma Life Sciences) and Alexa Fluor 647 Goat anti-Mouse IgG (Sigma Life Sciences) at 2 μg mL^{-1} for 45 min. After washing with PBS, the cells were mounted with mounting media containing 4′,6-diamidino-2-phenylindole (DAPI) for nuclei staining. Confocal microscopy images were acquired using a Zeiss laser scanning microscope (LSM 510) and processed using LSM 5 Release 4.2 software.

Statistical Analysis: For the DMT modulus, 2 scans were performed at different locations along the fibrillized collagen of each specimen. Each scan generated 512×512 data points for Young's modulus. For each property map, 10 regions of interest (ROIs) were selected and the median value was used to represent the property value for that ROI. Thus, for each group, 100 values (2 scans × 10 ROIs × 5 samples) were generated. Since normality (Shapiro–Wilk test) and homoscedasticity assumptions (modified Levene test) of the data for each parameter were violated, statistical analysis was performed by Kruskal–Wallis analysis of variance at $\alpha = 0.05$.

For cell titer and ALP activity, values (at least triplicate) were averaged and expressed as means ± standard deviation (SD). The statistical differences were determined using analysis of variance (ANOVA). The differences were considered statistically significant at $\alpha = 0.05$.

Supporting Information

Supporting Information is available from the Wiley Online Library or from the author.

Acknowledgements

[1] H. Gao, B. Ji, I. L. Jäger, E. Arzt, P. Fratzl, *Proc. Natl. Acad. Sci. USA* **2003**, *100*, 5597.

[2] M. Balooch, S. Habelitz, J. H. Kinney, S. J. Marshall, G. W. Marshall, *J. Struct. Biol.* **2008**, *162*, 404.

[3] L. A. Arsenault, *Bone Miner.* **1989**, *6*, 165.

[4] W. J. Landis, K. J. Hodgens, J. Arena, M. J. Song, B. F. McEwen, *Microsc. Res. Techn.* **1996**, *33*, 192.

[5] L. M. Siperko, W. J. Landis, *J. Struct. Biol.* **2001**, *135*, 313.

[6] E. P. Katz, S. T. Li, *J. Mol. Biol.* **1973**, *80*, 1.

[7] M. J. Olszta, X. Cheng, S. S. Jee, R. Kumar, Y. Y. Kim, M. J. Kaufman, E. P. Douglas, L. B. Gower, *Mater. Sci. Eng. R.* **2007**, *58*, 77.

[8] X. Su, K. Sun, F. Z. Cui, W. J. Landis, *Bone* **2003**, *32*, 150.

[9] E. A. McNally, H. P. Schwarcz, G. A. Botton, A. L. Arsenault, *PLoS One* **2012**, *7*, e29258.

[10] B. Alexander, T. L. Daulton, G. M. Genin, J. Lipner, J. D. Pasteris, B. Wopenka, S. Thomopoulos, *J. R. Soc. Interface* **2012**, *9*, 1774.

[11] J. H. Bradt, M. Mertig, A. Teresiak, W. Pompe, *Chem. Mater.* **1999**, *11*, 2694.

[12] W. Zhang, S. S. Liao, F. Z. Cui, *Chem. Mater.* **2003**, *15*, 3221.

[13] T. T. Thula, F. Svedlund, D. E. Rodriguez, J. Podschun, L. Pendi, L. B. Gower, *Polymers* **2011**, *3*, 10.

[14] E. Beniash, R. A. Metzler, R. S. Lam, P. U. Gilbert, *J. Struct. Biol.* **2009**, *166*, 133.

[15] J. Mahamid, A. Sharir, L. Addadi, S. Weiner, *Proc. Natl. Acad. Sci. USA* **2008**, *105*, 12748.

[16] A. George, A. Veis, *Chem. Rev.* **2008**, *108*, 4670.

[17] E. K. Girija, Y. Yokogawa, F. Nagata, *J. Mater. Sci. Mater. Med.* **2004**, *15*, 593.

[18] I. E. Chesnick, J T. Mason, A. A. Giuseppetti, N. Eidelman, K. Potter, *Biophys. J.* **2008**, *95*, 2017.

[19] A. S. Deshpande, E. Beniash, *Cryst. Growth Des.* **2008**, *8*, 3084.

[20] S. S. Jee, T. T. Thula, L. B. Gower, *Acta. Biomater.* **2010**, *6*, 3676.

[21] F. Nudelman, K. Pieterse, A. George, P. H. Bomans, H. Friedrich, L. J. Brylka, P. A. Hilbers, G. de With, N. A. Sommerdijk, *Nat. Mater.* **2010**, *9*, 1004.

[22] N. Nassif, F. Gobeaux, J. Seto, E. Belamie, P. Davidson, P. Panine, G. Mosser, P. Fratzl, M. M. Giraud-Guille, *Chem. Mater.* **2010**, *22*, 3307.

[23] T. T. Thula, D. E. Rodriguez, M. H. Lee, L. Pendi, J. Podschun, L. B. Gower, *Acta. Biomater.* **2011**, *7*, 3158.

[24] G. He, S. Gajjeraman, D. Schultz, D. Cookson, C. Qin, W. T. Butler, J. Hao, A. George, *Biochemistry* **2005**, *44*, 16140.

[25] S. Gajjeraman, K. Narayanan, J. Hao, C. Qin, A. George, *J. Biol. Chem.* **2007**, *282*, 1193.

[26] Y. Liu, Y. K. Kim, L. Dai, N. Li, S. O. Khan, D. H. Pashley, F. R. Tay, *Biomaterials* **2011**, *32*, 1291.

[27] Y. Liu, N. Li, Y. P. Qi, L. Dai, T. E. Bryan, J. Mao, D. H. Pashley, F. R. Tay, *Adv. Mater.* **2011**, *23*, 975.

[28] Y. K. Kim, L. S. Gu, T. E. Bryan, J. R. Kim, L. Chen, Y. Liu, J. C. Yoon, L. Breschi, D. H. Pashley, F. R. Tay, *Biomaterials* **2010**, *31*, 6618.

[29] D. K. Dubey, V. Tomar, *Appl. Phys. Lett.* **2010**, *96*, 023703.

[30] A. J. Hodge, J. A. Petruska, in *Aspects of Protein Structure*, (Ed. G. N. Ramachandran), Academic Press, New York, **1963**, pp. 289.

[31] K. E. Kadler, D. F. Holmes, J. A. Trotter, J. A. Chapman, *Biochem. J.* **1996**, *316*, 1.

[32] W. W. Leow, W. Hwang, *Langmuir* **2011**, *27*, 10907.

[33] W. Traub, T. Arad, S. Weiner, *Proc. Natl. Acad. Sci. USA* **1989**, *86*, 9822.

[34] W. J. Landis, K. J. Hodgens, J. Arena, M. J. Song, B. F. McEwen, *Microsc. Res. Techn.* **1996**, *33*, 192.

[35] G. He, T. Dahl, A. Veis, A. George, *Nat. Mater.* **2003**, *2*, 552.

[36] B. Pittenger, N. Erina, C. Su, *Bruker Application Note #128*, **2011**.

[37] K. Sweers, K. van der Werf, M. Bennink, V. Subramaniam, *Nanoscale Res. Lett.* **2011**, *6*, 270.

www.MaterialsViews.com

ADVANCED
FUNCTIONAL
MATERIALS
www.afm-journal.de

FULL PAPER

[38] T. J. Young, M. A. Monclus, T. L. Burnett, W. R. Broughton, S. L. Ogin, P. A. Smith, *Meas. Sci. Technol.* **2011**, *22*, 125703.

[39] B. V. Derjaguin, V. M. Muller, Y. P. Toporov, J. *Colloid Interface Sci.* **1975**, *53*, 314.

[40] S. R. Elliott, R. A. Robinson, *J. Bone Jt. Surg. Am.* **1957**, *39*, 167.

[41] H. Trebacz, K. Wójtowicz, *Int. J. Biol. Macromol.* **2005**, *37*, 257.

[42] J. A. J. van der Rijt, K. O. van der Werf, M. L. Bennink, P. J. Dijkstra, J. Feijen, *Macromol. Biosci.* **2006**, *6*, 697.

[43] I. Jäger, P. Fratzl, *Biophys. J.* **2000**, *79*, 1737.

[44] H. S. Gupta, J. Seto, W. Wagermaier, P. Zaslansky, P. Boesecke, P. Fratzl, *Proc. Natl. Acad. Sci. USA* **2006**, *103*, 17741.

[45] G. R. Cointry, R. F. Capozza, M. A. Chiappe, S. Feldman, M. D. Meta, S. M. Daniele, N. M. Fracalossi, P. Reina, J. L. Ferretti, *J. Bone Miner. Metab.* **2005**, *23 Suppl*, 30.

[46] L. Dai, Y. P. Qi, L. N. Niu, Y. Liu, C. R. Pucci, S. W. Looney, J. Q. Ling, D. H. Pashley, F. R. Tay, *Cryst. Growth Des.* **2011**, *11*, 3504.

[47] C. Higuchi, N. Nakamura, H. Yoshikawa, K. Itoh, *J. Bone Miner. Metab.* **2009**, *27*, 158.

[48] B. Ohler, *Rev. Sci. Instrum.* **2007**, *78*, 063107.